Energy band engineering of InGaN/GaN multi-quantum-well solar cells via AlGaN electron- and hole-blocking layers

Xuanqi Huang, Hong Chen, Houqiang Fu, Izak Baranowski, Jossue Montes, Tsung-Han Yang, Kai Fu, Brendan P. Gunning, Daniel D. Koleske, and Yuji Zhao

Citation: Appl. Phys. Lett. **113**, 043501 (2018); doi: 10.1063/1.5028530
View online: https://doi.org/10.1063/1.5028530
View Table of Contents: http://aip.scitation.org/toc/apl/113/4
Published by the American Institute of Physics

Energy band engineering of InGaN/GaN multi-quantum-well solar cells via AlGaN electron- and hole-blocking layers

Xuanqi Huang,[1] Hong Chen,[1] Houqiang Fu,[1] Izak Baranowski,[1] Jossue Montes,[1] Tsung-Han Yang,[1] Kai Fu,[1] Brendan P. Gunning,[2] Daniel D. Koleske,[2] and Yuji Zhao[1,a)]
[1]*School of Electrical, Computer & Energy Engineering, Arizona State University, Tempe, Arizona 85287, USA*
[2]*Sandia National Laboratories, MS 0601, P.O. Box 5800, Albuquerque, New Mexico 87185-0601, USA*

(Received 12 March 2018; accepted 9 July 2018; published online 24 July 2018)

In this paper, we perform a comprehensive study on energy band engineering of InGaN multi-quantum-well (MQW) solar cells using AlGaN electron- and hole-blocking layers. InGaN MQW solar cells with AlGaN layers were grown by metalorganic chemical vapor deposition, and high crystal quality was confirmed by high resolution X-ray diffraction measurements. Time-resolved photoluminescence results showed that the carrier lifetime on the solar cells with AlGaN layers increased by more than 40% compared to that on the reference samples, indicating greatly improved carrier collections. The illuminated current-density (J–V) measurements further confirmed that the short-circuit current density (J_{sc}) of the solar cells also benefited from the AlGaN layer design and increased 46%. At room temperature, the InGaN solar cells with AlGaN layers showed much higher power conversion efficiency (PCE), by up to two-fold, compared to reference devices. At high temperatures, these solar cells with AlGaN layers also delivered superior photovoltaic (PV) performance such as PCE, J_{sc}, and fill factor than the reference devices. These results indicate that band engineering with AlGaN layers in the InGaN MQW solar cell structures can effectively enhance the carrier collection process and is a promising design for high efficiency InGaN solar cells for both room temperature and high temperature PV applications. *Published by AIP Publishing*. https://doi.org/10.1063/1.5028530

III-nitride (III-N) materials have seen huge success in both electronics[1–6] and optoelectronics,[7–16] including power diodes,[1–6] solid-state lighting,[7–12] and integrated photonics.[13–16] Ternary InGaN alloys, in particular, have emerged in recent years as promising candidates for photovoltaic (PV) applications,[17–22] especially for high temperature PV applications, terrestrial photovoltaic thermal (PVT) hybrid solar collector systems, space applications, and top cells in multi-junction (MJ) solar cells. III-N materials' suitability for these device applications arises from their unique intrinsic properties, such as tunable wide bandgaps, a high absorption coefficient, high thermal stability, and outstanding radiation resistance.[23,24] To date, rapid progress has been made in the development of InGaN solar cells, with major emphasis placed on improving material quality and avoiding polarization-related effects. As a result, various approaches have been reported that focus on the growth of InGaN absorbing layers and the consequent device performance.[25–31] These include the use of strained InGaN/GaN quantum wells,[25,26] the optimization of structural parameters,[27,28] the use of native GaN substrates,[29,30] growth on different GaN crystal orientations,[30,31] etc. These methods reveal the relation between material quality, structural integrity, and the corresponding PV properties of InGaN layers. For example, the employment of free-standing GaN substrates can substantially boost power conversion efficiency (PCE) of InGaN solar cells by reducing their dislocation densities.[26,27,29] Additionally, the polarization doping[32] and the adoption of nonpolar and semipolar GaN substrates[30] are also able to mitigate polarization-induced issues and facilitate carrier transport.

Nevertheless, compared to traditional III-V materials, research on InGaN solar cells is still in its early stages and their PV performance is still far from satisfactory. The research efforts in developing high efficiency InGaN solar cells have been mainly focused on improving the material crystal quality, optimizing the optical designs, and controlling the polarization effects. On the other hand, the engineering of energy bands of solar cells using higher bandgap layers to act as window layers (or back surface fields) has been demonstrated as an effective approach to improve the carrier collection efficiency of solar cells. Such an approach has already been successfully implemented in Si heterojunctions with intrinsic thin-layer (HIT) solar cells,[33] III-V solar cells,[34–36] and II-VI solar cells like CdTe[37] and chalcogenides.[38] However, tailoring electronic energy band profiles with higher bandgap layers has not yet been thoroughly investigated in InGaN solar cells.

In this work, we demonstrate InGaN multi-quantum-well (MQW) solar cell structures with AlGaN layers as electron- and hole-blocking layers. This energy band design leads to substantially increased carrier lifetimes in InGaN MQW solar cells and improved carrier collection dynamics. The illuminated current-density (J–V) and external quantum efficiency (EQE) characterizations showed significant improvements for the solar cells with AlGaN layers compared to those without, mainly due to the huge enhancement in the short-circuit current density (J_{sc}). At high temperatures up to 450 °C, those cells with the optimized AlGaN layers also surpassed the PV performance of the reference ones in

a)Yuji.Zhao@asu.edu.

TABLE I. Summary of structure designs and device performance of InGaN/GaN MQW solar cells.

Sample No.	p-GaN (nm)	p-$Al_{0.15}Ga_{0.85}N$ (nm)	n-$Al_{0.15}Ga_{0.85}N$ (nm)	MQW	V_{oc} (V)	J_{sc} (mA/cm^2)	FF (%)	Conversion efficiency (%)
Ref.	100	0	0	30 periods $In_{0.15}Ga_{0.85}N$	2.09	0.87	52.57	0.95
1A	100	5	0	(3 nm)/GaN (7 nm) MQW	2.18	1.36	59.27	1.77
1B	100	10	0		2.17	1.43	54.31	1.69
1C	100	5	5		2.15	1.31	59.70	1.66
2A	50	5	0		1.66	1.49	63.17	1.57
2B	150	5	0		2.15	1.27	59.04	1.62

terms of all key parameters. The detailed discussions are as follows.

The InGaN MQW solar cell structures were grown by conventional metal-organic chemical vapor deposition (MOCVD) on (0001) sapphires. The indium compositions in the MQWs were determined to be 15% by high resolution X-ray diffraction (HRXRD) and were further verified by photoluminescence (PL). The reference device structure consists of 2 μm Si-doped n-GaN ([Si] = 3×10^{18} cm^{-3}), 125 nm highly Si-doped n$^+$-GaN ([Si] = 2×10^{19} cm^{-3}), 30 periods of InGaN (3 nm)/GaN (7 nm) MQWs, 110 nm Mg-doped p-GaN, and a 10 nm highly Mg-doped p$^+$-GaN contact layer. In addition, five InGaN MQW solar cells (namely, 1A, 1B, 1C, 2A, and 2B) with different AlGaN layers were also grown, and the details of their structures are summarized in Table I. All structures have the same InGaN MQW active regions. Samples 1A and 1B have p-$Al_{0.15}Ga_{0.85}N$ layers of 5 nm and 10 nm, respectively, and no n-$Al_{0.15}Ga_{0.85}N$ layers. Sample 1C has 5 nm of both p- and n-$Al_{0.15}Ga_{0.85}N$ layers. Samples 2A and 2B have the same p-$Al_{0.15}Ga_{0.85}N$ layers as sample 1A but with different p-GaN layer thicknesses (50 nm for 2A and 150 nm for 2B).

After the MOCVD growth, the crystal qualities of the InGaN MQW solar cell samples were characterized by the HRXRD measurement using a PANalytical X'Pert Pro materials research X-ray diffractometer system with Cu Kα radiations. The transmission and reflectance spectra of unprocessed wafers were characterized with a LAMBDA 950/1050 UV/VIS/NIR Spectrophotometer from Perkin Elmer. The PL and time-resolved PL (TRPL) measurements at room temperature (RT) were performed using a home-made micro-PL system equipped with an incident 405 nm laser and a HORIBA spectrometer with a liquid nitrogen cooled CCD detector. After material and optical characterizations, these InGaN epi-structures were then processed into solar cell devices with 1 mm × 1 mm mesas using standard contact lithography and inductively coupled plasma (ICP) etching. 130 nm indium-tin-oxide (ITO) layers were deposited by dc-sputtering on top of the mesa as a current spreading layer with post-annealing in N_2/O_2 at 500 °C. Ti/Al/Ni/Au ring contacts and Ti/Pt/Au grid contacts were deposited around the perimeter and on the top of the mesa, respectively. Both metal contacts were deposited via electron beam evaporation. The schematic device structure of the fabricated InGaN MQW solar cells of sample 1C is shown in Fig. 1(a). Illuminated J–V measurements were taken using an Oriel Class A Solar Simulator at 1 sun condition under the AM1.5G spectrum. The EQE measurement data were collected using an Oriel QEPVSI quantum efficiency measurement system and calibrated with a reference Si photodetector. A Linkam HFS600-PB4 stage with the capability of heating samples up to 600 °C was used to perform the temperature-dependent measurements. More details on characterization, fabrication, and PV measurements can be found in Refs. 30 and 39.

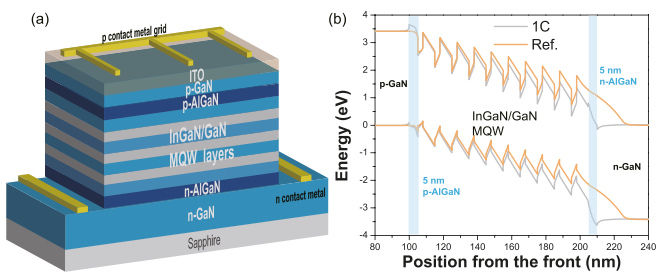

FIG. 1. (a) The schematic device structure of sample 1C and (b) the comparison of band diagrams between the reference sample and 1C.

Figure 1(b) shows the comparison of energy band structures in equilibrium between the reference structure and 1C. The energy band diagrams of InGaN MQW solar cells were simulated using TCAD Silvaco software. The detailed values of the confined ground states, band edges (at 100 nm and 210 nm), and the band offsets for electrons and holes with and without the p-AlGaN layer in the first and last quantum wells are presented in the supplementary material (see Tables S1 and S2). The employment of the p-$Al_{0.15}Ga_{0.85}N$ layer introduces a 0.297 eV increase in the conduction band offset while maintaining the same barrier height in the valence band. This enables more efficient extraction of holes to the p-GaN by blocking the overflowing electrons and reducing the recombination of electrons and holes in the p side. Likewise, the n-$Al_{0.15}Ga_{0.85}N$ layer lowers the conduction band offset by 0.634 eV and increases the valence band offset by 0.866 eV, enhancing electron transport to the n side. Therefore, both p- and n-$Al_{0.15}Ga_{0.85}N$ layers improve carrier collection and reduce the surface recombination near the contacts.

The growth and doping issues of AlGaN layers are very complicated and will negatively impact the performance of InGaN MQW solar cells if the crystal quality is low. Therefore, before the device characterization, we performed HRXRD ω-2θ scans across (0002) reflection for all the InGaN solar cell samples to analyze the material quality, and the results are shown in Fig. 2. The vertical dotted line indicates the main peak for GaN. The InGaN MQW peaks from the zeroth to the second order are well-distinguished and are located at nearly the same position. The indium compositions for all samples deduced from HRXRD results are ~15%. Overall, these results illustrate that all samples

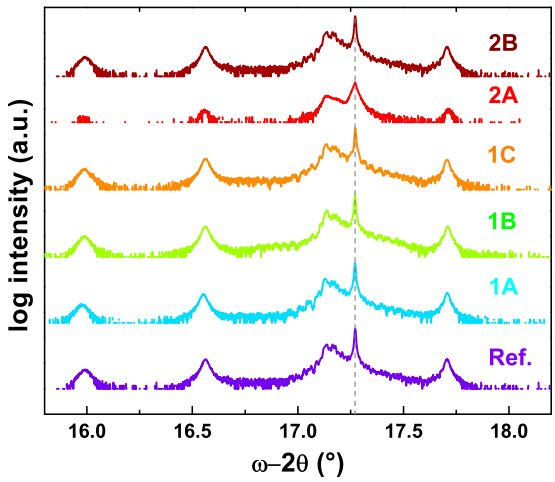

FIG. 2. The typical results of HRXRD ω-2θ scans taken across (002) reflection for sample ref., 1A, 1B, 1C, 2A, and 2B, respectively.

possess highly similar MQW structures without any negative effects caused by the addition of AlGaN layers. Additionally, the less obvious satellite peaks were found on sample 2A as shown in the XRD results. This is related to the less smooth interface between quantum wells and barriers, which leads to the slightly lower material quality in sample 2A.[40] Further investigations are being carried out to confirm this issue.

Figure 3 shows (a) the light absorption spectra, (b) the RT PL spectra, and (c) the RT TRPL results for all the InGaN MQW solar cell samples. The absorption spectra were determined from *Absorption* (λ) = *100% − Transmission* (λ) − *Reflection* (λ). The bandgap energies obtained from the absorption spectra and Tauc's plot (not shown here) were ~2.75 eV for all the 6 structures. This indicates an indium composition around 15%, which is in good agreement with the HRXRD results. Moreover, the emission peaks in PL measurements shown in Fig. 3(b) are in the range of 445–450 nm, which also correspond to both the HRXRD and absorption results. The normalized TRPL results at RT are presented in Fig. 3(c), and the carrier lifetimes fitted from exponential decay functions are also shown. The lifetime in the reference structure is only ~7.8 ns, while it is in the range from 11 to 16 ns for the other samples with AlGaN layers. A longer carrier lifetime indicates a higher possibility for photogenerated carriers to be collected at contacts.[41,42] Compared to the reference structure, those with AlGaN layers all exhibited significantly improved carrier lifetimes (>40%). This is due to the increased band bending in the quantum wells and thus reduced carrier recombination.[43] By comparing structures 1A and 1B, we can see that the thin p-AlGaN layer (5 nm) is preferred in solar cell design. This can be explained by fewer defects and/or dislocations being generated during the growth process. Additionally, a moderate thickness of the p-GaN layer (100 nm) leads to the longest lifetime among structures 1A, 2A, and 2B. This can be related to the tradeoff between the highly resistive nature of the p-GaN layer and material quality.

Figure 4 presents (a) the representative EQE spectra and (b) the illuminated *J*–*V* measurements for the samples. The cutoff edges of the EQE for all samples are almost the same at 450 nm, which is in good agreement with the absorption and PL results. Samples 1A to 2B all exhibited better EQE performance than the reference structure. The peak EQE for the reference sample is only ~47%, while it exceeded 60% for the other structures. The highest peak EQE of 65% was found in structure 2A. The large difference observed in EQE and internal quantum efficiency (IQE) (see Fig. S1) between the reference and other structures demonstrates that band engineering with AlGaN layers in InGaN MQW solar cells significantly enhanced the carrier collection efficiency, leading to better solar cell performance. Furthermore, for *J*–*V* curves, all InGaN solar cell structures with AlGaN layers (1A to 2B) exhibited markedly improved J_{sc} as expected. In contrast, all structures exhibited essentially the same open-circuit voltage (V_{oc}) values except 2A. More details on the comparison of *J*–*V* performance are discussed in the following paragraph.

Figure 5 shows the extracted values of key PV performance parameters of (a) V_{oc}, (b) J_{sc}, (c) fill factor (FF), and (d) PCE from *J*–*V* curves in the form of a box chart for the reference sample (ref.) and samples 1A, 1B, 1C, 2A, and 2B. These values are also included in Table I. The measurements were performed on ~10 devices for each structure and ~60 devices in total. The V_{oc} of ref. (2.09 V) is slightly smaller than those of 1A, 1B, 1C, and 2B. This is attributed to increased quasi-Fermi splitting for the solar cell samples with AlGaN layers. It is also worth noting that the voltage-bandgap offsets (W_{oc}) of 1A, 1B, 1C, and 2B are smaller than 0.6 V, which acts as an indicator of superior material quality in InGaN MQW solar cells.[22,44] Sample 2A showed

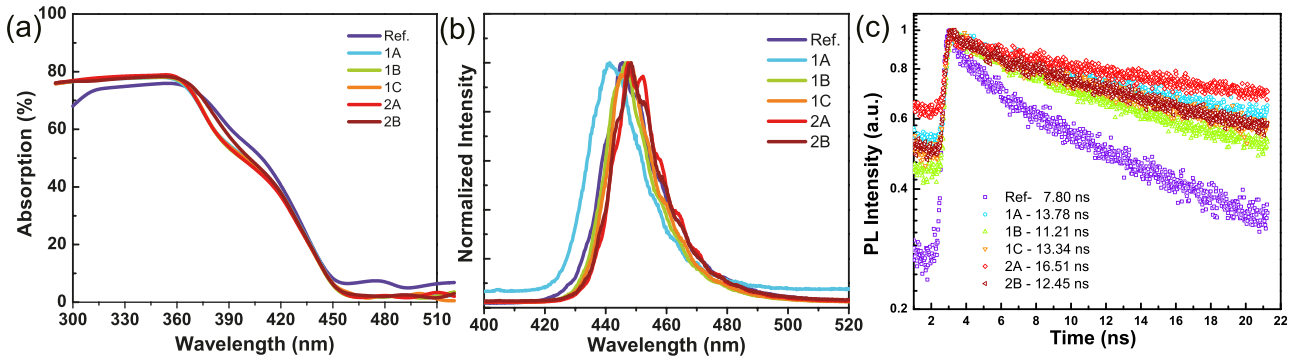

FIG. 3. (a) The light absorption spectra, (b) the room-temperature photoluminescence (PL) spectra, and (c) room-temperature time-resolved photoluminescence (TRPL) results for sample ref., 1A, 1B, 1C, 2A, and 2B, respectively.

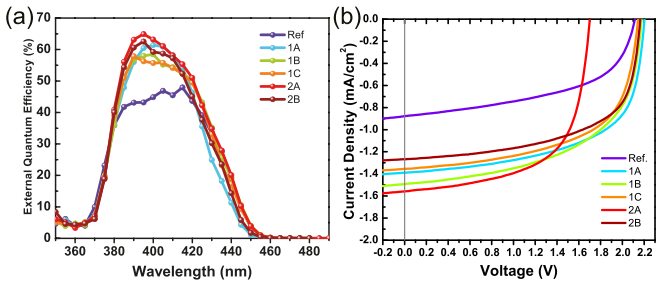

FIG. 4. (a) The representative EQE spectra and (b) the representative illuminated current density–voltage (J–V) measurements for sample ref., 1A, 1B, 1C, 2A, and 2B, respectively.

lower V_{oc} possibly due to the inferior material quality. Additionally, the J_{sc} value of the reference sample is only 0.87 mA/cm^2, while the values for samples with AlGaN layers are larger than 1.27 mA/cm^2, with an enhancement of more than 46%. The FF values of 1A to 2B range from 54% to 63%, while it is slightly lower in ref. (52.57%). As a result, the reference structure exhibited the lowest PCE of all (0.95%), which is largely limited by its J_{sc}. In contrast, samples 1A to 1C exhibited a significantly improved PCE of more than 1.6%, which demonstrates an increase of more than 68%. The best solar cell performance was achieved on sample 1A which exhibited a V_{oc} of 2.20 V, a J_{sc} of 1.39 mA/cm^2, a FF of 60.52%, and a corresponding PCE of 1.85% under 1 sun AM1.5G equivalent illumination. These results show the high potential of adopting AlGaN layers as an effective band engineering method to improve the PV performance of InGaN solar cells.

To further study the effects of AlGaN layers on the high temperature performance of InGaN solar cells, we performed high temperature J–V measurements ranging from 25 °C to 450 °C. Figure 6 presents the comparison of device parameters of normalized (a) conversion efficiency, (b) J_{sc}, (c) V_{oc}, and (d) FF between sample reference and 1C extracted from high temperature J–V measurements. To better compare the key device parameters at varying temperatures, we normalized each collection of parameters with the corresponding values of the reference at 25 °C. Other InGaN solar cell devices with AlGaN layers that are not shown here exhibited similar trends to sample1 C. Figure 6(a) shows that the efficiencies of 1C are much higher than that of the reference sample across the entire temperature range. It is worth noting that the difference in efficiencies between the two samples reduces as temperature increases. With an increase in temperature, the bandgap energies of AlGaN layers decrease and the thermionic emission rate of photogenerated carriers rises. Those two effects together result in the less pronounced enhancement effect originated from AlGaN layers. A similar trend was observed for J_{sc} values of the two samples as shown in Fig. 6(b). Furthermore, an increase of FF up to 300 °C was observed on both samples which is shown in Fig. 6(c). This rollover phenomenon in FF can be ascribed to the trade-off between carrier escape and recombination at high temperatures, which has also been identified in previous reports on InGaN/GaN MQW solar cells.[21,45] Finally, both devices showed the similar values and trends for V_{oc} as shown in Fig. 6(d). This similarity originated from the temperature-dependent behaviors of the intrinsic carrier concentration and essentially the bandgaps of III-nitrides.[46] Consequently, the reference InGaN solar cell samples shared many similarities in PV performance with previous reports.[21,22,45] Nevertheless, InGaN solar cells with AlGaN layers completely outperformed the reference solar cell samples in almost every aspect of PV performance across the entire temperature range in measurements.

In summary, we have performed the comprehensive study on energy band engineering of InGaN MQW solar cells using AlGaN electron- and hole-blocking layers and demonstrated that such an approach can effectively improve the PV performance of InGaN MQW solar cells. Energy band simulation and TRPL results showed that the carrier collection and carrier lifetime were improved significantly with the incorporation of AlGaN layers in the InGaN solar cells. The illuminated J–V measurements further confirmed that J_{sc} benefited most from this design and increased more

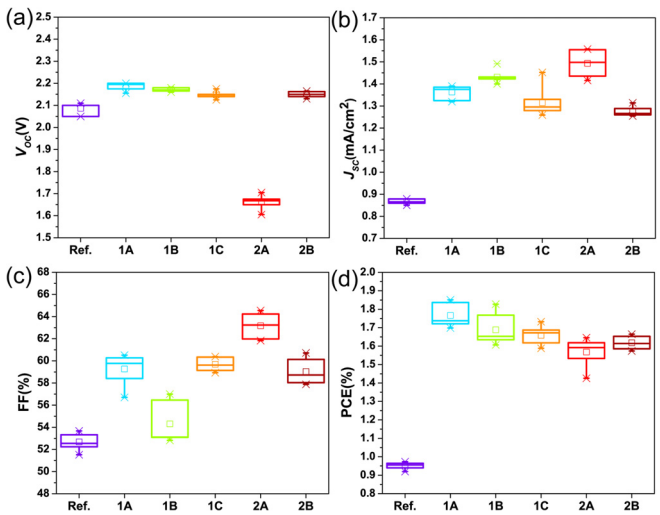

FIG. 5. The extracted values of (a) open-circuit voltage (V_{oc}), (b) short-circuit current (J_{sc}), (c) fill factor (FF), and (d) power conversion efficiency (PCE) from J–V curves for sample ref., 1A, 1B, 1C, 2A, and 2B, respectively.

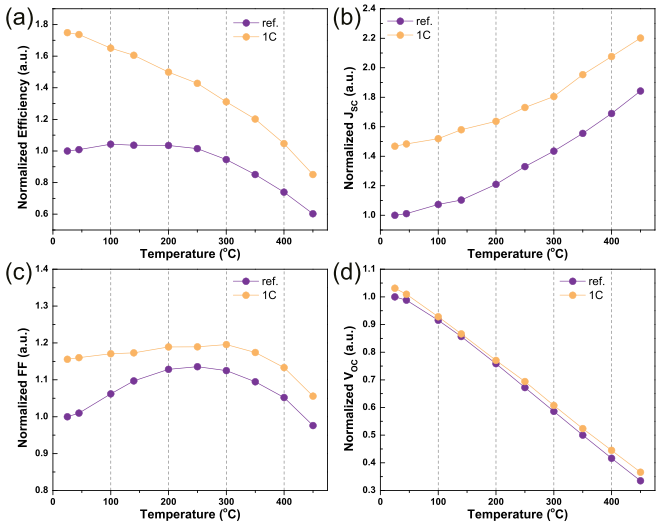

FIG. 6. The comparison of device parameters of normalized (a) power conversion efficiency, (b) short-circuit current (J_{sc}), (c) fill factor (FF), and (d) open-circuit voltage (V_{oc}) between the sample reference and 1C from high temperature J–V measurements.

than 46%. The PCE of the solar cell device with AlGaN layers almost doubled over the reference structure. At elevated temperatures, those with AlGaN layers also achieved better performance than the reference sample. These results demonstrate the feasibility and practicality of the adoption of AlGaN layers in the InGaN MQW solar cell structures for further improving the carrier collection process. This engineering of the energy band therefore has the full potential to enable high efficiency InGaN solar cells for both room temperature and high temperature applications.

See supplementary material for the detailed values of the confined ground states, band edges (at 100 nm and 210 nm), and the band offsets for electrons and holes with and without the p-AlGaN layer in the first and last quantum wells (Tables S1 and S2) and the internal quantum efficiency (IQE) spectra for sample ref., 1A, 1B, 1C, 2A, and 2B, respectively (Fig. S1).

This work was supported by an Early Career Faculty grant from NASA's Space Technology Research Grants Program. The authors would like to express sincere gratitude to Professor Yong-Hang Zhang for access to his optoelectronics characterization laboratory. The authors would also like to thank Dr. Lin Gan for PL and TRPL measurements and Professor Cun-Zheng Ning for access to his optical characterization laboratory. We gratefully acknowledge the use of facilities within the LeRoy Eyring Center for Solid State Science and Nanofab at Arizona State University.

[1]H. Fu, X. Huang, H. Chen, Z. Lu, X. Zhang, and Y. Zhao, IEEE Electron Device Lett. **38**, 763 (2017).
[2]D. Disney, H. Nie, A. Edwards, D. Bour, H. Shah, and I. C. Kizilyalli, in *25th International Symposium on Power Semiconductor Devices ICs (ISPSD)* (2013), pp. 59–62.
[3]M. Qi, K. Nomoto, M. Zhu, Z. Hu, Y. Zhao, V. Protasenko, B. Song, X. Yan, G. Li, J. Verma, S. Bader, P. Fay, H. G. Xing, and D. Jena, Appl. Phys. Lett. **107**, 232101 (2015).
[4]H. Ohta, N. Kaneda, F. Horikiri, Y. Narita, T. Yoshida, T. Mishima, and T. Nakamura, IEEE Electron Device Lett. **36**, 1180 (2015).
[5]H. Fu, X. Huang, H. Chen, Z. Lu, I. Baranowski, and Y. Zhao, Appl. Phys. Lett. **111**, 152102 (2017).
[6]D. Ji, C. Gupta, A. Agarwal, S. H. Chan, C. Lund, W. Li, S. Keller, U. K. Mishra, and S. Chowdhury, IEEE Electron Device Lett. **39**(5) 1 (2018).
[7]S. Nakamura, T. Mukai, and M. Senoh, Appl. Phys. Lett. **64**, 1687 (1994).
[8]Y. Zhao, S. Tanaka, C.-C. Pan, K. Fujito, D. Feezell, J. S. Speck, S. P. DenBaars, and S. Nakamura, Appl. Phys. Express **4**, 082104 (2011).
[9]R. M. Farrell, E. C. Young, F. Wu, S. P. DenBaars, and J. S. Speck, Semicond. Sci. Technol. **27**, 024001 (2012).
[10]Z. Lu, P. Tian, H. Chen, I. Baranowski, H. Fu, X. Huang, J. Montes, Y. Fan, H. Wang, X. Liu, R. Liu, and Y. Zhao, Opt. Express **25**, 17971 (2017).
[11]S. P. DenBaars, D. Feezell, K. Kelchner, S. Pimputkar, C.-C. Pan, C.-C. Yen, S. Tanaka, Y. Zhao, N. Pfaff, R. Farrell, M. Iza, S. Keller, U. Mishra, J. S. Speck, and S. Nakamura, Acta Mater. **61**, 945 (2013).
[12]H. Chen, H. Fu, Z. Lu, X. Huang, and Y. Zhao, Opt. Express **24**, A856 (2016).
[13]C. Xiong, W. Pernice, K. K. Ryu, C. Schuck, K. Y. Fong, T. Palacios, and H. X. Tang, Opt. Express **19**, 10462 (2011).
[14]H. Chen, H. Fu, X. Huang, X. Zhang, T.-H. Yang, J. A. Montes, I. Baranowski, and Y. Zhao, Opt. Express **25**, 31758 (2017).
[15]N. V. Triviño, U. Dharanipathy, J.-F. Carlin, Z. Diao, R. Houdré, and N. Grandjean, Appl. Phys. Lett. **102**, 081120 (2013).
[16]H. Chen, X. Huang, H. Fu, Z. Lu, X. Zhang, J. A. Montes, and Y. Zhao, Appl. Phys. Lett. **110**, 181110 (2017).
[17]X. Zheng, R.-H. Horng, D.-S. Wuu, M.-T. Chu, W.-Y. Liao, M.-H. Wu, R.-M. Lin, and Y.-C. Lu, Appl. Phys. Lett. **93**, 261108 (2008).
[18]A. G. Bhuiyan, K. Sugita, A. Hashimoto, and A. Yamamoto, IEEE J. Photovoltaics **2**, 276 (2012).
[19]N. G. Toledo and U. K. Mishra, J. Appl. Phys. **111**, 114505 (2012).
[20]X. Huang, H. Fu, H. Chen, Z. Lu, D. Ding, and Y. Zhao, J. Appl. Phys. **119**, 213101 (2016).
[21]Z. Chen, X. Zheng, Z. Li, P. Wang, X. Rong, T. Wang, X. Yang, F. Xu, Z. Qin, W. Ge, B. Shen, and X. Wang, Appl. Phys. Lett. **109**, 062104 (2016).
[22]J. J. Williams, H. McFavilen, A. M. Fischer, D. Ding, S. Young, E. Vadiee, F. A. Ponce, C. Arena, C. B. Honsberg, and S. M. Goodnick, IEEE J. Photovoltaics **7**, 1646 (2017).
[23]J. Wu, W. Walukiewicz, K. M. Yu, W. Shan, J. W. A. Iii, E. E. Haller, H. Lu, W. J. Schaff, W. K. Metzger, and S. Kurtz, J. Appl. Phys. **94**, 6477 (2003).
[24]J. Wu, J. Appl. Phys. **106**, 011101 (2009).
[25]R. M. Farrell, C. J. Neufeld, S. C. Cruz, J. R. Lang, M. Iza, S. Keller, S. Nakamura, S. P. DenBaars, U. K. Mishra, and J. S. Speck, Appl. Phys. Lett. **98**, 201107 (2011).
[26]Y. Kuwahara, T. Fujii, T. Sugiyama, D. Iida, Y. Isobe, Y. Fujiyama, Y. Morita, M. Iwaya, T. Takeuchi, S. Kamiyama, I. Akasaki, and H. Amano, Appl. Phys. Express **4**, 021001 (2011).
[27]N. G. Young, R. M. Farrell, Y. L. Hu, Y. Terao, M. Iza, S. Keller, S. P. DenBaars, S. Nakamura, and J. S. Speck, Appl. Phys. Lett. **103**, 173903 (2013).
[28]S. Valdueza-Felip, A. Mukhtarova, L. Grenet, C. Bougerol, C. Durand, J. Eymery, and E. Monroy, Appl. Phys. Express **7**, 032301 (2014).
[29]Y. Kuwahara, T. Fujii, Y. Fujiyama, T. Sugiyama, M. Iwaya, T. Takeuchi, S. Kamiyama, I. Akasaki, and H. Amano, Appl. Phys. Express **3**, 111001 (2010).
[30]X. Huang, H. Fu, H. Chen, X. Zhang, Z. Lu, J. Montes, M. Iza, S. P. DenBaars, S. Nakamura, and Y. Zhao, Appl. Phys. Lett. **110**, 161105 (2017).
[31]J. Bai, Y. P. Gong, Z. Li, Y. Zhang, and T. Wang, Sol. Energy Mater. Sol. Cells **175**, 47 (2018).
[32]C. J. Neufeld, S. C. Cruz, R. M. Farrell, M. Iza, J. R. Lang, S. Keller, S. Nakamura, S. P. DenBaars, J. S. Speck, and U. K. Mishra, Appl. Phys. Lett. **98**, 243507 (2011).
[33]K. Masuko, M. Shigematsu, T. Hashiguchi, D. Fujishima, M. Kai, N. Yoshimura, T. Yamaguchi, Y. Ichihashi, T. Mishima, N. Matsubara, T. Yamanishi, T. Takahama, M. Taguchi, E. Maruyama, and S. Okamoto, IEEE J. Photovoltaics **4**, 1433 (2014).
[34]C. Zhang, Y. Kim, C. Ebert, N. N. Faleev, and C. B. Honsberg, in *2015 IEEE 42nd Photovoltaic Specialist Conference* (*PVSC*) (2015), pp. 1–5.
[35]M. Vaisman, S. Fan, K. Nay Yaung, E. Perl, D. Martín-Martín, Z. J. Yu, M. Leilaeioun, Z. C. Holman, and M. L. Lee, ACS Energy Lett. **2**, 1911 (2017).
[36]S. Essig, C. Allebé, T. Remo, J. F. Geisz, M. A. Steiner, K. Horowitz, L. Barraud, J. S. Ward, M. Schnabel, A. Descoeudres, D. L. Young, M. Woodhouse, M. Despeisse, C. Ballif, and A. Tamboli, Nat. Energy **2**(9) (2017).
[37]Y. Zhao, M. Boccard, S. Liu, J. Becker, X.-H. Zhao, C. M. Campbell, E. Suarez, M. B. Lassise, Z. Holman, and Y.-H. Zhang, Nat. Energy **1**, 16067 (2016).
[38]P. Reinhard, A. Chirilă, P. Blösch, F. Pianezzi, S. Nishiwaki, S. Buechelers, and A. N. Tiwari, in *IEEE 38th Photovoltaic Specialists Conference* (*PVSC*) *PART 2* (2012), pp. 1–9.
[39]X. Huang, H. Fu, H. Chen, Z. Lu, I. Baranowski, J. Montes, T.-H. Yang, B. P. Gunning, D. Koleske, and Y. Zhao, Appl. Phys. Lett. **111**, 233511 (2017).
[40]A. M. Yong, C. B. Soh, X. H. Zhang, S. Y. Chow, and S. J. Chua, Thin Solid Films **515**, 4496 (2007).
[41]S. Liu, Q. Wang, H. Xiao, K. Wang, C. Wang, X. Wang, W. Ge, and Z. Wang, Superlattices Microstruct. **109**, 194 (2017).
[42]L. Redaelli, A. Mukhtarova, A. Ajay, A. Núñez-Cascajero, S. Valdueza-Felip, J. Bleuse, C. Durand, J. Eymery, and E. Monroy, Jpn. J. Appl. Phys., Part 1 **54**, 072302 (2015).
[43]H. Fu, Z. Lu, X. H. Zhao, Y. H. Zhang, S. P. DenBaars, S. Nakamura, and Y. Zhao, J. Disp. Technol. **12**, 736 (2016).
[44]R. R. King, D. Bhusari, A. Boca, D. Larrabee, X.-Q. Liu, W. Hong, C. M. Fetzer, D. C. Law, and N. H. Karam, Prog. Photovoltaics: Res. Appl. **19**, 797 (2011).
[45]L. Zhao, T. Detchprohm, and C. Wetzel, Appl. Phys. Lett. **105**, 243903 (2014).
[46]P. Singh and N. M. Ravindra, Sol. Energy Mater. Sol. Cells **101**, 36 (2012).